Journal of The Electrochemical Society, **151** (3) A358-A367 (2004)
0013-4651/2004/151(3)/A358/10/$7.00 © The Electrochemical Society, Inc.

Electron Transport in PEFCs

Hua Meng and Chao-Yang Wang*,z

Electrochemical Engine Center and Department of Mechanical and Nuclear Engineering, The Pennsylvania State University, University Park, Pennsylvania 16802, USA

A three-dimensional, single-phase, isothermal numerical model of polymer electrolyte fuel cell (PEFC) was employed to investigate effects of electron transport through the gas diffusion layer (GDL) for the first time. An electron transport equation was additionally solved in the catalyst and gas diffusion layers, as well as in the current collector. It was found that the lateral electronic resistance of GDL, which is affected by the electronic conductivity, GDL thickness, and gas channel width, played a critical role in determining the current distribution and cell performance. Under fully-humidified gas feed in the anode and cathode, both oxygen and lateral electron transport in GDL dictated the current distribution. The lateral electronic resistance dominated the current distribution at high cell voltages, while the oxygen concentration played a more decisive role at low cell voltages. With reduced GDL thickness, the effect of the lateral electronic resistance on the current distribution and cell performance became even stronger, because the cross-sectional area of GDL for lateral electron transport was smaller. Inclusion of GDL electron transport enabled the thickness of GDL and widths of the gas channel and current collecting land to be optimized for better current distribution and cell performance. In addition, the present model enables: (*i*) direct incorporation of contact resistances emerging from GDL/catalyzed membrane or GDL/land interface, (*ii*) implementation of the total current as a more useful boundary condition than the constant cell voltage, and (*iii*) stack modeling with cells connected in series and hence having the identical total current.
 [DOI: 10.1149/1.1641036]

Manuscript submitted June 13, 2003; revised manuscript received September 15, 2003. Available electronically January 26, 2004.

The polymer electrolyte fuel cell (PEFC) is a promising alternative power plant for transportation because of its high energy efficiency, low emission, and low noise. In the past decade, numerical modeling and simulation has become increasingly important for enhancing physical understanding and optimizing engineering design and operation of PEFCs. In recently developed three-dimensional (3-D) PEFC models, computational fluid dynamics (CFD) methodology has been employed to integrate electrochemical processes with water/proton cotransport in the PE to enable multiphysics modeling and large-scale simulation.[1-7] In these numerical models, the conservation equations of mass, momentum, and species were typically solved with source/sink terms arising from electrochemical kinetics. In the models of Dutta *et al.*[2,3] the membrane-electrode assembly (MEA) was not included in the computational domain but simplified as an interface without thickness. As such, water and proton transport across MEA were treated using simple linear relationships as in the early work of Nguyen and White.[8] Since the electrochemical and transport phenomena inside MEA are critically important for PEFC performance, detailed MEA submodels were considered in other 3-D PEFC simulations.[1,4-7] In the large-scale numerical investigation of PEFC performances under both fully-humidified gas feed and low-humidity operation,[6,7] it was found that the ionic resistances in the anode and cathode catalyst layers were comparable to that in the membrane, further demonstrating that the catalyst layers cannot be neglected in PEFC modeling.

In all the 3-D PEFC models published to date, electron transport in the catalyst and gas diffusion layers, and in the current collector is ignored by assuming a sufficiently large electronic conductivity and consequently, constant electronic phase potential in these materials. This assumption is valid likely in the current collector in the through-plane direction, of which the electronic conductivity is of the order of 20,000 S/m for graphite plates, but could be largely inappropriate in the gas diffusion and catalyst layers, in which the effective electronic conductivities range only from 300 to 500 S/m (in the through-plane direction). Since the typical thickness of the gas diffusion layer (GDL) is 300 μm and the typical half-width of the gas channel is 500 μm, the through-plane electronic resistance across GDL and the lateral electronic resistance across the half width of the gas channel are both around 10 $m\Omega\ cm^2$. These electronic resistances could significantly change the current distribution, both macroscopically along the flow direction and mesoscopically between the channel and land areas. Although the electron transport equation was solved in the 1-D PEFC models of Bernardi and Verbrugge,[9,10] the lateral electronic resistance can only be assessed in a 3-D geometry. Furthermore, solving the electron transport equation results in the following additional advantages: (*i*) enabling direct incorporation of the contact resistance at interfaces between two mating components in the solution process; (*ii*) enabling direct implementation of the total current as a boundary condition instead of the cell voltage; and (*iii*) enabling stack modeling with cells connected in series.

In this paper, a 3-D isothermal, electrochemical and transport fully coupled PEFC model is described. The complete set of conservation equations of mass, momentum, and species are solved numerically with proper account of electrochemical kinetics. An electron transport equation is included in the catalyst and gas diffusion layers, and in the current collector in order to investigate the effects of electronic resistance in GDL. A proton transport equation is solved inside MEA to accurately account for electrolyte ionic resistance. The effects of the lateral electronic resistance on the current distribution and cell performance are studied in detail for the first time.

Numerical Model

In this section, a 3-D single-phase, isothermal numerical model of PEFC is presented, which is capable of investigating electrochemical and transport phenomena in all nine regions of a PEFC, namely the gas channels, diffusion and catalyst layers, and the current collectors on both anode and cathode sides, and the membrane. Conservation equations of mass, momentum, chemical species, proton and electron transport, as presented in Table I (Eq. 1-7) are numerically solved, with proper account of electrochemical kinetics. Superficial velocities are used in the momentum equations in order to automatically ensure mass flux continuity at the interface between the porous GDL and nonporous gas channel.

The mass and momentum equations are numerically solved to obtain the flow field. The source terms in the momentum equations are added based on the Darcy's law, representing an extra drag force proportional to fluid viscosity and velocity, and inversely proportional to the permeability of a porous medium. The species concentration equations are solved to obtain hydrogen, oxygen, and water distributions, in which the source terms are implemented based on electrochemical kinetics. A proton conservation equation is solved inside MEA, giving accurate account of ionic resistance in these regions.

* Electrochemical Society Active Member.
z E-mail: cxw31@psu.edu

Table I. Conservation equations.

	Conservation equations		Source terms
Mass	$\nabla \cdot (\rho \mathbf{u}) = 0$	1	
Momentum	$\frac{1}{\varepsilon^2}\nabla \cdot (\rho \mathbf{u}\mathbf{u}) = -\nabla p + \nabla \cdot \tau + S_u$	2	in diffusion and catalyst layers: $S_u = -\frac{\mu}{K}\mathbf{u}$
Species concentration	$\nabla \cdot (\mathbf{u}c_i) = \nabla \cdot (D_i^{eff}\nabla c_i) + S_i$	3	in catalyst layers: $S_i = -\frac{s_i j}{nF}$ except water $S_i = -\nabla \cdot \left(\frac{n_d}{F}\mathbf{i}\right) - \frac{s_i j}{nF}$ for water in MEA
Proton	$\nabla \cdot (\kappa^{eff}\Delta\phi_e) + S_\phi = 0$	4	in catalyst layers: $S_\phi = j$
Electron	$\nabla \cdot (\sigma_s^{eff}\nabla\phi_s) + S_\phi = 0$	5	in catalyst layers: $S_\phi = -j$

Electrochemical reactions

$$\sum_i s_i M_i = ne^-$$

where $\begin{cases} M_i \equiv \text{chemical formula of species} \\ s_i \equiv \text{stoichiometry coefficient} \\ n \equiv \text{number of electrons transfered} \end{cases}$

Hydrogen oxidation reaction in anode side: $H_2 - 2H^+ = 2e^-$ 6

Oxygen reduction reaction in cathode side: $2H_2O - O_2 - 4H^+ = 4e^-$ 7

An additional electron transport equation, Eq. 5 in Table I is solved numerically in the catalyst and gas diffusion layers, and in the current collector on both anode and cathode sides in order to fully investigate electronic transport in GDL and its effect on the current distribution and cell performance. The source terms in both anode and cathode catalyst layers correspond to the hydrogen oxidation and oxygen reduction reactions, creating or consuming electrons. Note also that electrons always flow from a low potential to a high potential point.

Electrochemical reactions in a PEFC, including the hydrogen oxidation reaction (HOR) and oxygen reduction reaction (ORR), are treated using proper source/sink terms in the species concentration, and proton and electron transport equations. The transfer current densities in these equations are expressed by the linear and Tafel approximations of Butler-Volmer equation in the anode and cathode, respectively, as follows

$$\text{Anode} \quad j = aj_{0,a}^{ref}\left(\frac{c_{H_2}}{c_{H_2,ref}}\right)^{1/2}\left(\frac{\alpha_a + \alpha_c}{RT}F\eta\right) \qquad [8]$$

$$\text{Cathode} \quad j = aj_{0,c}^{ref}\left(\frac{c_{O_2}}{c_{O_2,ref}}\right)\exp\left(-\frac{\alpha_c}{RT}F\eta\right) \qquad [9]$$

where all the parameters are described in Table II. On the anode side, the Butler-Volmer equation is linearized based on the fact of facile HOR kinetics or small overpotential. The overpotentials are defined as

$$\text{Anode side} \quad \eta = \phi_s - \phi_e \qquad [10]$$

$$\text{Cathode side} \quad \eta = \phi_s - \phi_e - U_{oc} \qquad [11]$$

where U_{oc} is the open-circuit potential defined as[11]

$$U_{oc} = 1.23 - 0.9 \times 10^{-3}(T - 298) + \frac{RT}{2F}\left(\ln p_{H_2} + \frac{1}{2}\ln p_{O_2}\right) \qquad [12]$$

The electronic and electrolyte phase potentials, ϕ_s and ϕ_e, are determined by solving the electron and proton transport equations, Eq. 4 and 5 in Table I as discussed later in this section.

Water transport caused by electro-osmotic drag is treated as an extra source/sink term in the water concentration equation, Eq. 3, where i_e is the local current density vector (similar to that defined in Eq. 21 in a vector form) and n_d stands for the electro-osmotic drag coefficient[12,13]

$$n_d = \begin{cases} 1.0 & \text{for } \lambda \leqslant 14 \\ 1.5/8(\lambda - 14) + 1.0 & \text{otherwise} \end{cases} \qquad [13]$$

The water concentration in the membrane is defined as

$$c_w^m = \frac{\rho_{dry}\lambda}{EW} \qquad [14]$$

Table II. Electrochemical and transport parameters.

Anode total exchange current density, aj_0 (A/m^3)	1×10^9
Cathode total exchange current density, aj_0 (A/m^3)	1×10^4
Reference hydrogen concentration, C_{H_2} (mol/m^3)	40
Reference oxygen concentration, C_{O_2} (mol/m^3)	40
Anode transfer coefficient	$\alpha_a = \alpha_c = 1$
Cathode transfer coefficient	$\alpha_c = 1$
Faraday constant, F	96487
Porosity of diffusion layer	0.6
Porosity of catalyst layer	0.112
Volume fraction of ionomer in catalyst layer	0.4
Permeability of the diffusion layer (m^2)	1×10^{-15}
Equivalent weight of ionomer (kg/mol)	1.1
Dry membrane density (kg/m^3)	1980
Universal gas constant (J/mol K)	8.314
Electronic conductivity in current collector (S/m)	20000
Effective electronic conductivity in GDL (S/m)	300-500
Cell temperature (°C)	80
Anode/cathode pressure (atm)	2/2
Anode/cathode stoichiometry (1 A/cm^2)	2/2

Table III. Physicochemical relations.

Description	Equation	Unit
Transfer current density	8 9	 A/m^3
Overpotential	10 11	 V
Open-circuit potential	12	V
Electro-osmotic drag coefficient	13	
Water concentration in membrane	14	mol/m^3
Water activity	15	
Water saturation pressure	16	atm
Water content	17	
Membrane water diffusivity	18	m^2/s
Proton conductivity	19	S/m
Effective diffusivity/conductivity	20	m^2/s

where ρ_{dry} and EW represent the dry membrane density and its equivalent molecular weight, respectively.

Membrane water content, defined as water molecules per sulfonic-acid group (SO_3^-), is determined by the water activity at the interface of membrane and gas phases in thermodynamic equilibrium. Water activity in the gas phase is calculated by

$$a = \frac{C_w RT}{p^{sat}} \quad [15]$$

where the saturation pressure of water was fitted to tabular data using the following expression[14]

$$\log_{10} p^{sat} = -2.1794 + 0.02953(T - 273.15) - 9.1837 \times 10^{-5}(T - 273.15)^2 + 1.4454 \times 10^{-7}(T - 273.15)^3 \quad [16]$$

An empirical formulation,[14] correlating membrane water content with water activity, is employed in this model, in which the existence of liquid water is considered using a linear relationship above water activity of unity

$$\lambda = \begin{cases} 0.043 + 17.18a - 39.85a^2 + 36.0a^3 & 0 < a \leqslant 1 \\ 14 + 1.4(a - 1) & 1 < a \leqslant 3 \end{cases} \quad [17]$$

Membrane water diffusivity is calculated using the following relationship of Motupally *et al.*[15]

$$D_w^m = \begin{cases} 3.1 \times 10^{-7}\lambda(e^{0.28\lambda} - 1)e^{[-2346/T]} & 0 < \lambda \leqslant 3 \\ 4.17 \times 10^{-8}\lambda(1 + 161e^{-\lambda})e^{[-2346/T]} & \text{otherwise} \end{cases} \quad [18]$$

A charge conservation equation, Eq. 4 in Table I, is solved to describe proton transport inside MEA. The dependence of proton conductivity on water content is calculated using the following empirical expression of Springer *et al.*[14]

$$\kappa = (0.5139\lambda - 0.326)\exp\left[1268\left(\frac{1}{303} - \frac{1}{T}\right)\right] \quad [19]$$

The electron transport equation, Eq. 5 in Table I, is solved to obtain the electronic phase potential in the catalyst and gas diffusion layers, and in the current collector. Various electronic conductivity values are listed in Table II.

The effective mass diffusivity and proton conductivity in porous media are described using the Bruggeman relation

$$D_i^{eff} = D_i\varepsilon^{1.5}, \quad \kappa^{eff} = \kappa\varepsilon^{1.5} \quad [20]$$

Local current density in the membrane is calculated by

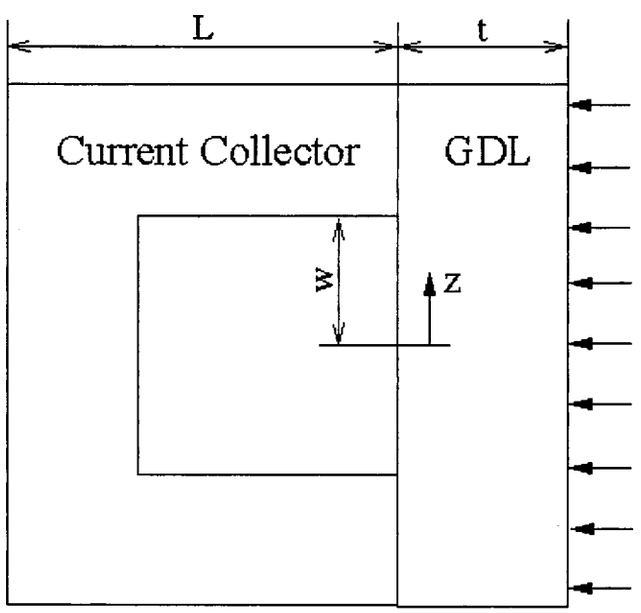

Figure 1. Schematic of the current collecting land and GDL.

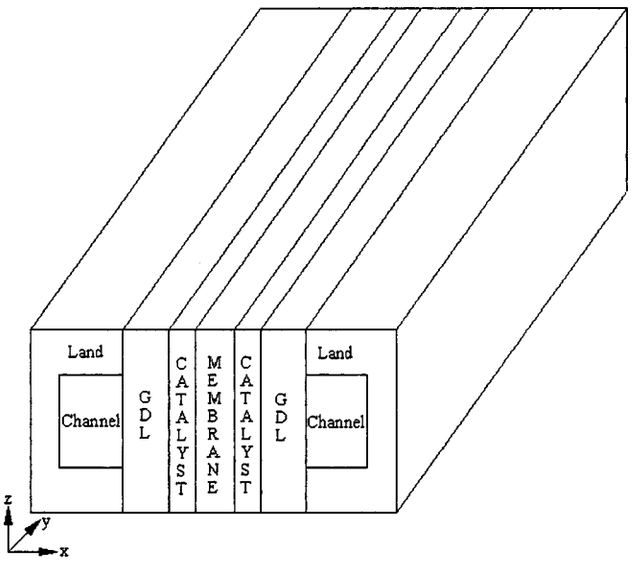

Figure 2. Geometry of a single straight-channel PEFC.

Table IV. Cell geometry.

Fuel cell geometry [mm]		
Cell length		100
Gas channel	Depth	1
	Width	1
Layer thickness	Diffusion	0.3
	Catalyst	0.01
	Membrane	0.025
Land width		0.5
Computational cell numbers		~310,000

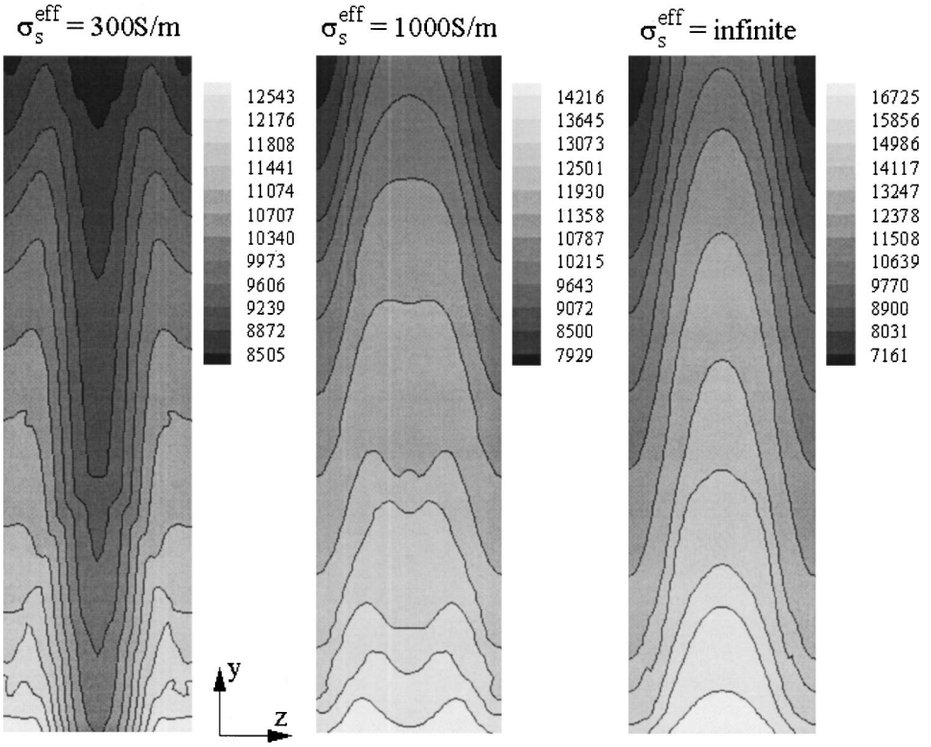

Figure 3. Ionic current distributions (A/m^2) in the middle of membrane under different electronic conductivities in GDL (at 0.65 V).

$$I = -\kappa^{eff}\nabla\phi_e \quad [21]$$

The average current density over the membrane area is given by

$$I_{avg} = \frac{1}{A}\int_A IdA \quad [22]$$

where I is the local current density on the membrane and A is the membrane area.

The conservation equations and their supplemental relationships are summarized in Tables I and III, respectively. The present PEFC numerical model is implemented into a commercial CFD package, Fluent, basing on its user-coding capability.[16]

Results and Discussion

Theoretical analysis.—Figure 1 presents a schematic of the current collector and GDL. The typical thickness of the current collector (L) is 1,000 μm, the thickness of the GDL (t) is 300 μm, and the half-width of the gas channel (w) is 500 μm. The effective electronic conductivities of the current collector and GDL (assumed isotropic for simplicity) are assumed to be 20,000 and 300 S/m, respectively. The typical electronic resistance in the current collector (R_1) is thus derived as

$$R_1 = \frac{L}{\sigma_{land}} = \frac{1000\ \mu m}{20000\ S/m} = 0.5\ m\Omega\ cm^2 \quad [23]$$

The electronic resistance in the current collector is small, and therefore, negligible. The through-plane ohmic resistance across GDL in the direction perpendicular to the membrane (R_2) is

$$R_2 = \frac{t}{\sigma_s^{eff}} = \frac{300\ \mu m}{300\ S/m} = 10\ m\Omega\ cm^2 \quad [24]$$

The lateral electronic resistance through the half-width of the gas channel (R_3) is

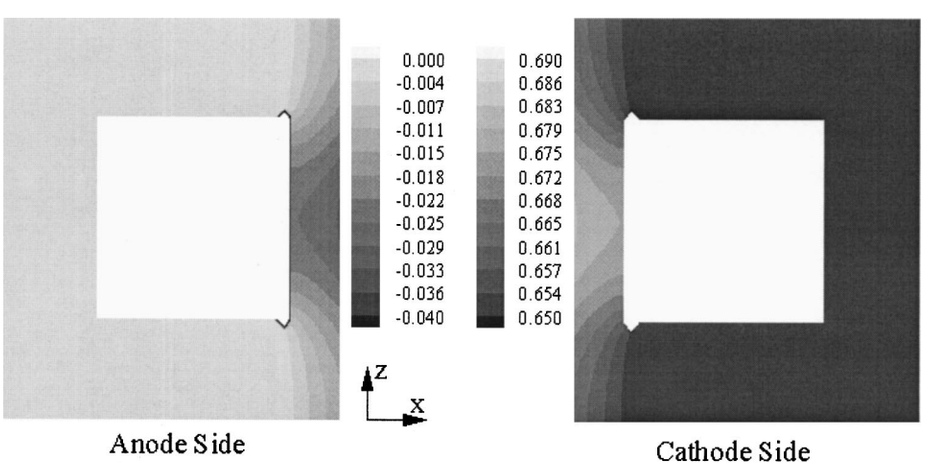

Figure 4. Electronic phase potential (V) distribution in the current collecting land and GDL on the anode and cathode sides.

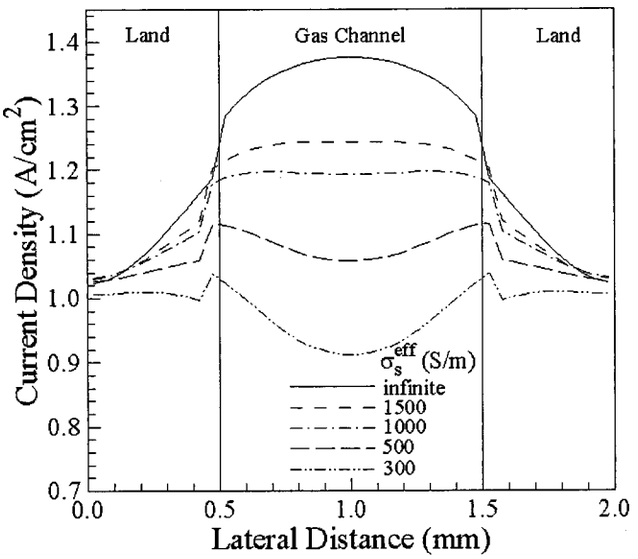

Figure 5. Ionic current distributions in the lateral direction in the mid-length of the cell at different electronic conductivities in GDL (GDL thickness: 300 μm).

$$R_3 = \frac{w}{\sigma_s^{\text{eff}}} = \frac{500\ \mu\text{m}}{300\ \text{S/m}} = 16.7\ \text{m}\Omega\ \text{cm}^2 \qquad [25]$$

The electronic phase potential variation is proportional to both electronic resistance and average current density. Since the average current densities in the through-plane and lateral directions are different, the electronic resistances in the two directions, R_2 and R_3, are not directly comparable. Assuming that the average current density under the gas channel is a constant $\bar{I}$, and the average current density through the GDL thickness (t) is uniform, the lateral electronic phase potential variation in GDL can then be derived as

$$\Delta\phi_s = \int_0^w \frac{\bar{I}z}{t}\frac{dz}{\sigma_s^{\text{eff}}} = \bar{I}R_3\frac{w}{2t} \qquad [26]$$

A scaling factor should, therefore, be included in the lateral electronic resistance. The modified lateral electronic resistance is

$$R_3' = R_3\frac{w}{2t} = 16.7\frac{500\ \mu\text{m}}{600\ \mu\text{m}} = 13.9\ \text{m}\Omega\ \text{cm}^2 \qquad [27]$$

The through-plane and lateral electronic resistances (R_2 and R_3') are sufficiently large to affect the current distribution, both globally on the cell level and locally between individual channel and land in the in-plane direction.

The parameter $w/2t$ in Eq. 26, *i.e.*, the ratio of the half width of the gas channel to the doubled GDL thickness, is therefore an important variable in PEFC design. At a given gas channel width, the lateral electronic phase potential variation will increase when decreasing the GDL thickness. Numerical results presented in the next section reveal that the current density under the gas channel decreased with decreasing the GDL thickness, causing highly nonuniform current distribution. It is evident from the present analysis that the GDL in PEFC functions not only to distribute reactants to the catalyst layer but also to provide a path for lateral electron conduction.

Numerical results and discussion.—The effects of the lateral electron transport on current distribution and cell performance are numerically investigated using a single straight-channel PEFC, as shown in Fig. 2. The cell geometry is described in Table IV. Careful grid independence study has been conducted to ensure accurate numerical results. A total of 316,800 computational cells were found to be sufficient in the present numerical simulations. The FC is operated at 80°C and 2 atm with fully humidified hydrogen and air fed into the anode and cathode inlet, respectively. The stoichiometry on both sides is set at two, based on the reference current density of 1 A/cm^2. The electronic potential in the y-z plane on the anode side ($x = 0$) is defined as zero, while it is set equal to the cell voltage on the cathode side.

As shown in Eq. 25 and 27, the lateral electronic resistance is determined by the electronic conductivity, GDL thickness, and gas channel width. A parametric study is conducted to find out its effect on current distribution and cell performance. The variation of the lateral electronic resistance is presently carried out through changing the GDL conductivity. The effect should be the same through changing the GDL thickness and/or the gas channel width. Current distributions in the midthickness of the membrane under three different electronic conductivities of GDL are presented in Fig. 3. For the electronic conductivity of 300 S/m, the maximum current density is located under the edges between the gas channel and the current collecting land as this location offers the best combination of easy access by oxygen and a short path for electron transport onto the land. Here, the lateral electron transport in GDL plays a critical role in determining the current distribution locally between channel and land. Figure 4 shows the corresponding electronic phase potential distribution in the current collector and GDL. Because of the lateral electronic resistance, the minimum electronic potential occurs under the middle of the GDL on the anode side, while the maximum appears under the middle of the GDL on the cathode side, resulting in the lowest overpotentials and hence slowest electrochemical reactions there. Numerical results indicate that the width of the gas channel and current collecting land are key optimization parameters for better cell performance.

In Fig. 3, as the electronic conductivity increases to 1,000 S/m, the current density under the middle of the gas channel starts to increase because oxygen supply becomes more critical at higher electronic conductivity. Over the second portion of the cell, the maximum current density occurs under the middle of the gas channel, dominated by oxygen concentration. By assuming an infinitely large electronic conductivity, *i.e.*, completely neglecting electron transport, oxygen supply becomes the sole factor determining the current distribution, and as a result, the maximum current density always occurs under the middle of the gas channel.

Current distributions along the in-plane direction in the midlength of the cell under different electronic conductivities of GDL are presented in Fig. 5. In order to neglect lateral electron

Table V. Average current density with various GDL electronic conductivity.

GDL thickness (300 μm)			GDL thickness (100 μm)		
Electron conductivity (S/m)	Average current density (A/cm^2)	Relative error (%)	Electron conductivity (S/m)	Average current density (A/cm^2)	Relative error (%)
∞	1.23	-	∞	1.23	-
1,500	1.17	4.9	5,000	1.19	3.3
1,000	1.14	7.3	2,000	1.15	6.5
500	1.08	12.2	1,000	1.09	11.4
300	1.00	18.7	300	0.95	22.8

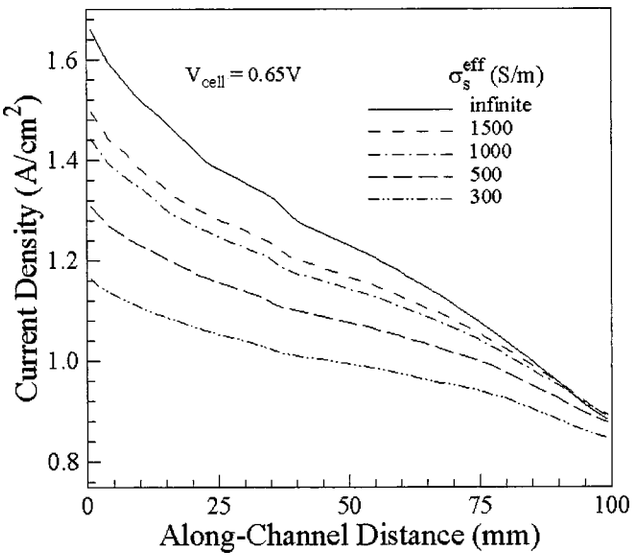

Figure 6. Current distributions in the middle of the membrane in the along-channel direction at different electronic conductivities in GDL.

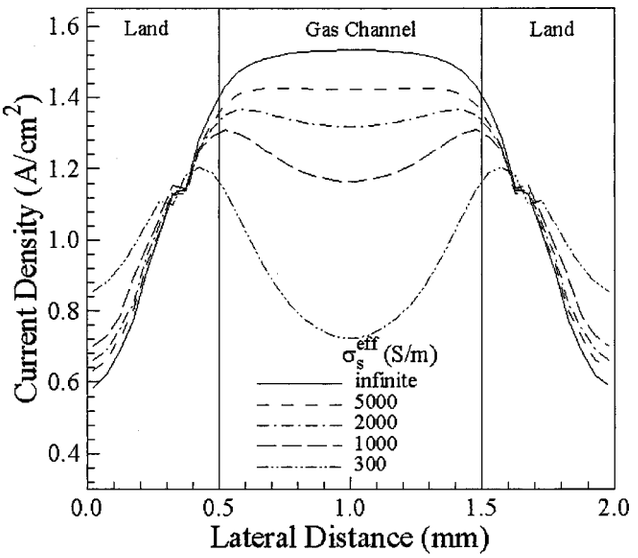

Figure 7. Ionic current distribution in the lateral direction in the middle of the cell at different electronic conductivities in GDL (GDL thickness: 100 μm).

transport, the electronic conductivity of GDL has to reach at least 1,500 S/m, at which the relative error of the average current density is about 5% as compared with the average current density assuming an infinitely large electronic conductivity. The average current densities at different electronic conductivities in GDL are listed and compared in Table V.

Electronic resistance in GDL will not only affect the current distribution in the lateral direction, but also that in the along-channel direction. Current distributions in the middle of membrane under different electronic conductivities in GDL in the along-channel direction are presented in Fig. 6. At a low electronic conductivity, the current distribution in the membrane becomes more uniform, but at a decreased average value. This trend is in accordance with the common belief that when an FC operation is dominated more by ohmic resistance, its overall performance is low but the current distribution is more uniform as the ohmic resistance is homogeneous. Because of the GDL electronic resistance, the current density near the channel inlet is reduced significantly. However, the decrease of the current density near the channel end is small because more oxygen is still available there.

The effect of GDL thickness on electronic phase potential distribution and cell performance is shown in Fig. 7, where the GDL thickness is decreased to 100 μm. With a thinner GDL, although oxygen can get access to the catalyst layer more easily, the cross-sectional area of the GDL for lateral electron transport, on the other hand, becomes smaller. As shown in Fig. 7, the effect of the lateral electronic resistance becomes more significant at a given electronic conductivity, compared with the results in Fig. 5. In this case, the electronic resistance can only be neglected for GDL electronic conductivity greater than 5,000 S/m. Numerical results clearly show the two important roles played by GDL in a PEFC: distributing reactant and product, and transporting electrons in the lateral direction onto the current collector. Therefore, the property of GDL should be optimized not only to improve reactant permeation and product water removal, but also to provide more effective electron conduction and more uniform current distribution.

Variations in the current distribution in both along-channel and lateral directions are presented in Fig. 8 for a GDL electronic conductivity of 300 S/m and a cell voltage of 0.65 V. While the electronic conductivity of 300 S/m is typical in the through-plane direction, it could be much higher in the in-plane direction because the GDL material is highly anisotropic. The present case thus represents a high-resistance limiting situation. The current distribution in the lateral direction near the channel inlet (*i.e.*, $y/y_0 = 0.1$ where y is the axial distance along the channel) indicates strong effect of lateral electron transport, because sufficient oxygen is available in the catalyst layer under both gas channel and land. The minimum current density in this case is under the middle of the gas channel and increase toward the land. Close to the cell outlet (*i.e.*, $y/y_0 = 0.9$), because oxygen is largely consumed, the situation changes dramatically. In this case, current distribution in the lateral direction becomes more uniform. Although the minimum current density still appears under the middle of the gas channel, the maximum current density also occurs under the gas channel region. With further decrease of oxygen concentration toward the land, the current density experiences a sharp decrease. Under the land area, the current density also decreases toward the edge because oxygen concentration is lowest there. Figure 9 illustrates current density distributions in the

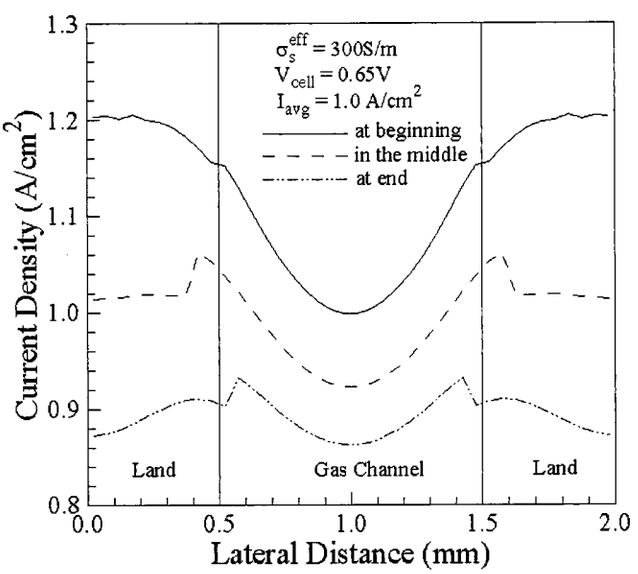

Figure 8. Current distributions in the middle of the membrane in both along-channel and lateral directions (0.65 V and 300 S/m).

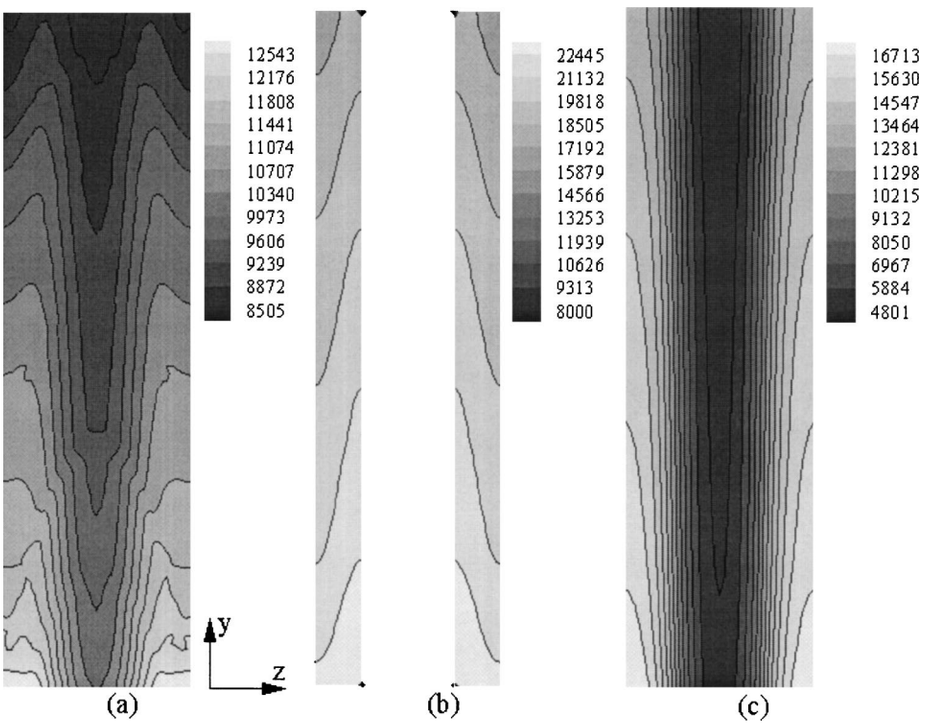

Figure 9. (a) Ionic current distribution (A/m^2) in the middle of the membrane, and electronic current distribution in (b) the two lands bounding the gas channel, and (c) inside the base surface of the current collector (0.65 V and 300 S/m).

middle of the membrane, in the land above and below the gas channel, and in the outside land. Because of existence of the gas channel, the current distribution is highly nonuniform even in the outside land, where the electronic conductivity is 20,000 S/m. Typical distributions of electron and proton phase potentials are presented in Fig. 10. Cathode overpotential in this case is around 400 mV, which is significantly larger than that on the anode side.

Current distributions in the middle of the membrane in both along-channel and lateral directions at two different cell voltages are compared in Fig. 11-12. In Fig. 11, lateral electronic resistance dominates the current distribution at a high cell voltage of 0.8 V. In this case, the minimum current density always occurs under the middle of the gas channel and increases towards the land. At a low cell voltage of 0.5 V, oxygen concentration plays a decisive role in determining the current distribution. Except at the very beginning of the cell inlet, where oxygen concentration is sufficiently high everywhere within the catalyst layer, the maximum current density always occurs under the middle of the gas channel and decreases towards the land.

By solving the electron transport equation, the contact resistance in a PEFC can be directly incorporated in the solution process. This is an important feature because the contact resistance between GDL and the catalyst layer is generally not a constant; it is larger under the gas channel than under the land. Fig. 13 shows the electron

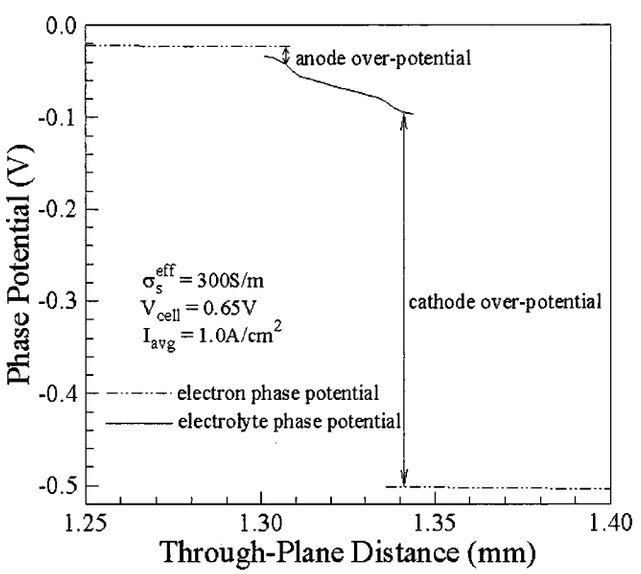

Figure 10. Variation of electronic and electrolyte phase potentials (0.65 V and 300 S/m).

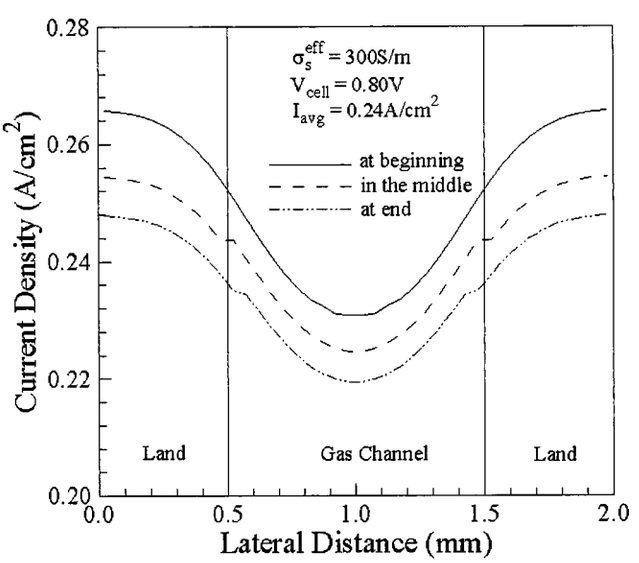

Figure 11. Current variation in the middle of the membrane in both along-channel and lateral directions (0.8 V and 300 S/m).

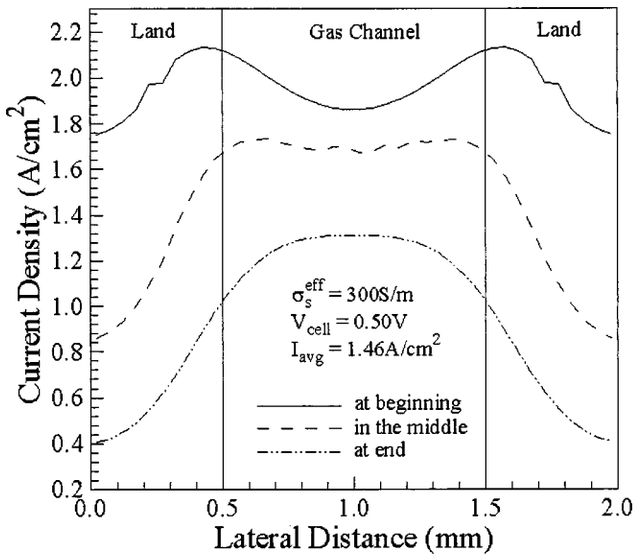

Figure 12. Current variation in the middle of the membrane in both along-channel and lateral directions (0.5 V and 300 S/m).

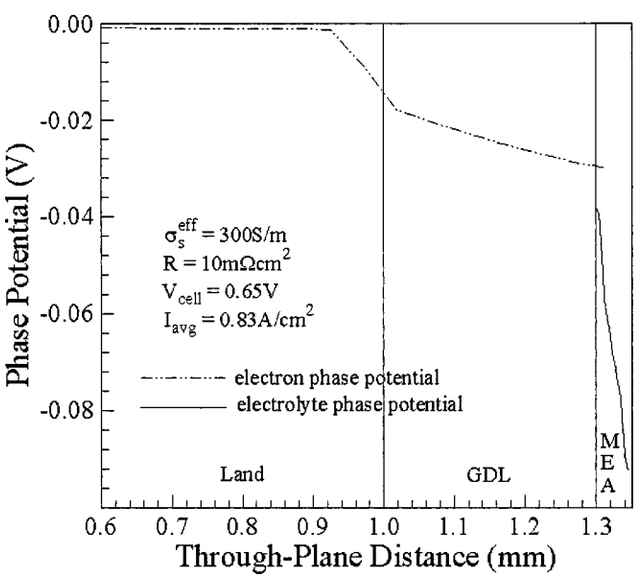

Figure 13. Electronic phase potential variation in the current collector and GDL with a contact resistance of 10 mΩ cm^2 (0.65 V and 300 S/m).

phase potential variation in the current collector and GDL with a constant contact resistance of 10 mΩ cm^2 added between the current collecting land and GDL. The existence of contact resistance is indicated in Fig. 13 by the sudden change of the electronic phase potential at that interface. Figure 14 illustrates the distribution of electronic phase potential on both anode and cathode sides in a PEFC. The abrupt variation of the electronic potential between the current collecting land and GDL reflects the effect of contact resistance.

Figure 15 shows that variations in the electronic phase potentials in catalyst layers on both anode and cathode sides are almost identical. Since the electronic phase potential variation is determined by the electronic resistance and current distribution, and electronic resistances are the same on both anode and cathode sides, it indicates that the current distributions are the same on the two sides. This phenomenon is related to the 1-D proton transport across the membrane, which can also be observed in Fig. 4 and 14. This result can, therefore, serve as a convergence criterion in the numerical calculation.

Conclusions

A 3-D, single-phase, isothermal numerical model of PEFC was developed, which is capable of investigating electrochemical and transport phenomena in all nine regions of a PEFC, namely the gas channels, diffusion and catalyst layers, and the current collectors on both anode and cathode sides, and the membrane. The complete set of conservation equations of mass, momentum, species, and charge (both protons and electrons) are numerically solved with proper account of electrochemical kinetics. The electron transport equation is solved in the catalyst and gas diffusion layers, and in the current collector, enabling numerical investigation of the lateral electronic resistance in GDL for the first time.

A single straight-channel PEFC is numerically studied in detail, with focus on the impact of the lateral electron transport on the current distribution and cell performance. It was found that the lateral electronic resistance of GDL, which was affected by the electronic conductivity, GDL thickness, and gas channel width, played a critical role in determining the current distribution and cell performance. With the fully-humidified inlet gases on both anode and cathode sides, the current distribution was determined by two factors: oxygen supply and lateral electronic resistance in GDL. At a high cell voltage, the lateral electronic resistance dictated the current distribution. In this case, the minimum current density always occurred under the middle of the gas channel and increased toward the current collecting land. At a low cell voltage, however, oxygen concentration played a dominant role in determining the current distribution. Except at the inlet section of the cell, where oxygen concentration was sufficiently high everywhere within the catalyst layer, the maximum current density always occurred under the middle of the gas channel and decreased towards the land.

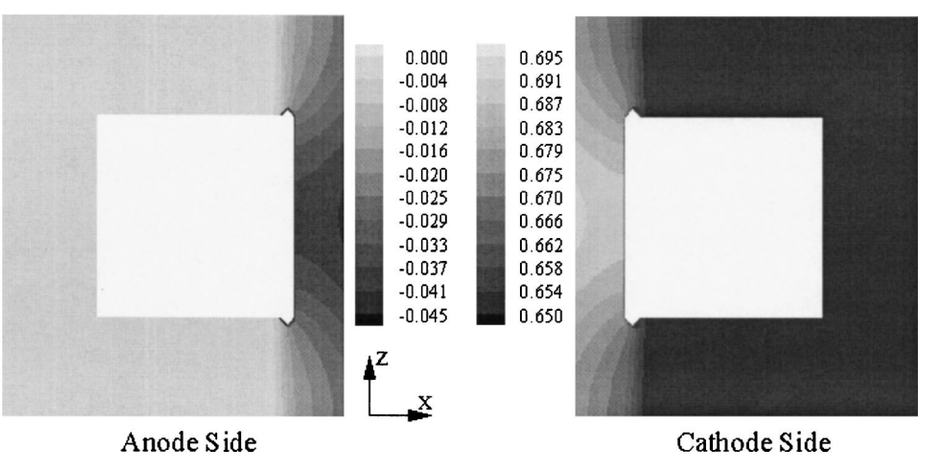

Figure 14. Electronic phase potential distribution in the current collector and GDL with a contact resistance of 10 mΩ cm^2 (0.65 V and 300 S/m).

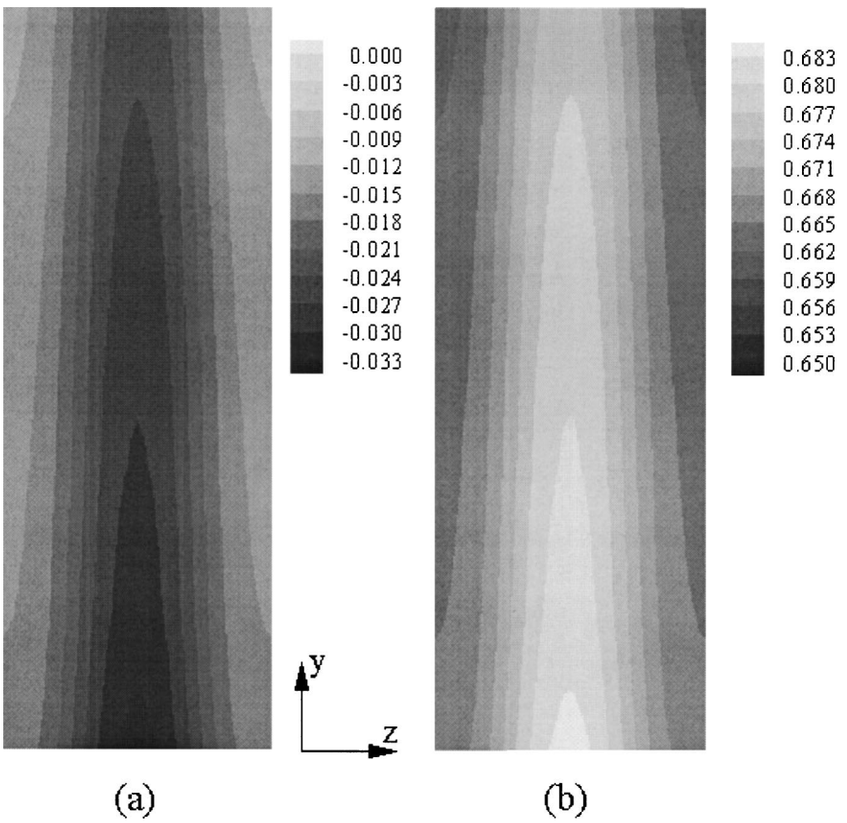

Figure 15. Electronic phase potential distributions in catalyst layers on (a) the anode and (b) the cathode sides.

When the thickness of GDL decreased, the effect of the lateral electronic resistance on the current distribution and cell performance became even stronger, because the cross-sectional area of GDL for lateral electron transport became smaller. Numerical results indicated that the gas diffusion layer in a PEFC serves two important functions: reactant distribution and lateral electron transport. Therefore, the thickness of GDL could be optimized for better current distribution and cell performance. In addition, the widths of the gas channel and the current collecting land could also be optimized.

Solving the electron transport equation gives rise to additional advantages. The contact resistance can now be directly incorporated in the solution. The constant current boundary condition can also be easily implemented in a PEFC model. This enables stack modeling with many cells connected in series and hence requiring constant current across all cells. Finally, it is straightforward to extend the present work to account for anisotropy of electron transport that is commonly found in FC GDL.

Acknowledgments

Funding for this work from DOE ultraclean fuel program under cooperative agreement no. DE-FC26-01NT41098 is acknowledged.

Penn State University assisted in meeting the publication costs of this article.

List of Symbols

a	water activity
c	molar concentration, mol/m^3
D	mass diffusivity, m^2/s
EW	equivalent weight of dry membrane, kg/mol
F	Faraday constant, 96487 C/mol
i	current density vector, A/m^2
j	transfer current density, A/m^3
K	permeability, m^2
M_w	molecular weight, kg/mol
n	number of electrons in electrochemical reaction
n_d	electro-osmotic drag coefficient
p	pressure, Pa
R	universal gas constant, 8.314 J/(mol K)
S	source term in transport equation
s	stoichiometry coefficient in electrochemical reaction
T	temperature, K
u	fluid velocity and superficial velocity in porous medium, m/s
U_{oc}	open-circuit potential, V

Greek

α	transfer coefficient
ε	porosity
η	overpotential, V
Φ	phase potential, V
κ	proton conductivity, S/m
λ	water content in membrane
μ	viscosity, kg/(m s)
ρ	density, kg/m^3
σ	electronic conductivity, S/m

Superscripts

eff	effective value in a porous medium
m	membrane
ref	reference value
sat	saturation value

Subscripts

a	anode
c	cathode
e	electrolyte
i	species index
m	mixture or membrane
oc	open circuit
s	electron
w	water

References

1. S. Um, C. Y. Wang, and K. S. Chen, *J. Electrochem. Soc.*, **147**, 4485 (2000).
2. S. Dutta, S. Shimpalee, and J. W. Van Zee, *J. Appl. Electrochem.*, **30**, 135 (2000).
3. S. Dutta, S. Shimpalee, and J. W. Van Zee, *Int. J. Heat Mass Transfer*, **44**, 2029 (2001).
4. T. Zhou and H. Liu, *Int. Transport Phenomena*, **3**, 177 (2001).
5. S. Um and C. Y. Wang, *J. Power Sources*, **125**, 40 (2004).
6. H. Meng and C. Y. Wang, *Chem. Eng. Sci.*, Submitted.
7. H. Meng and C. Y. Wang, *Chem. Eng. Sci.*, Submitted.
8. T. V. Nguyen and R. E. White, *J. Electrochem. Soc.*, **140**, 2178 (1993).
9. D. M. Bernardi and M. W. Verbrugge, *AIChE J.*, **37**, 1151 (1991).
10. D. M. Bernardi and M. W. Verbrugge, *J. Electrochem. Soc.*, **139**, 2477 (1992).
11. C. Berger, *Handbook of Fuel Cell Technology*, Prentice-Hall, Englewood Cliffs, NJ (1968).
12. T. A. Zawodzinski, J. Davey, J. Valerio, and S. Gottesfeld, *Electrochim. Acta*, **40**, 297 (1995).
13. F. N. Büchi and G. G. Scherer, *J. Electrochem. Soc.*, **148**, A183 (2001).
14. T. E. Springer, T. A. Zawodzinski, and S. Gottesfeld, *J. Electrochem. Soc.*, **138**, 2334 (1991).
15. S. Motupally, A. J. Becker, and J. W. Weidner, *J. Electrochem. Soc.*, **147**, 3171 (2000).
16. Fluent 6.0 UDF Manual, Fluent Inc. (2001).